Zn2+ and Cu2+ doping of one-dimensional lead-free hybrid perovskite ABX3 for white light emission and green solar cell applications

H. Jellali, R. Msalmi, H. Smaoui, S. Elleuch, A. Tozri, Thierry Roisnel, E. Mosconi, N.A. Althubiti, H. Naïli

Zn^{2+} and Cu^{2+} doping of one-dimensional lead-free hybrid perovskite ABX_3 for white light emission and green solar cell applications

Hayet Jellali,[a] Rawia Msalmi,[b] Hichem Smaoui,[a] Slim Elleuch,[c] Anowar Tozri,[d] Thierry Roisnel,[e] Edoardo Mosconi,[f] Numa A. Althubiti [g] and Houcine Naïli [b]*

[a.] *Laboratory of materials for energy and environment, and modeling, Faculty of Sciences of Sfax, Sfax University, Tunisia.*

[b.] *Laboratory Physico Chemistry of the Solid State, Department of Chemistry, Faculty of Sciences of Sfax, Sfax University, Tunisia.*

[c.] *Laboratory of Applied Physic, Faculty of Sciences of Sfax, Sfax University, Tunisia*

[d.] *Physics Department, College of Science, Jouf University, Sakaka 2014, Saudi Arabia.*

[e.] *Uni Rennes, CNRS, ISCR (Institut des Sciences Chimiques de Rennes), UMR6226, 35000 Rennes, France.*

[f.] *Computational Laboratory for Hybrid/Organic Photovoltaics (CLHYO), Istituto CNR di Scienze e Tecnologie Chimiche "Giulio Natta" (CNR-SCITEC), Via Elce di Sotto 8, 06123 Perugia, Italy.*

[g.] *Chemistry department, College of Science, Jouf University, Sakaka 2014, Saudi Arabia.*

Corresponding Author

*Houcine Naïli: Email: Houcine_naili@yahoo.com

Highlights

- One-dimensional $DMACdCl_3$ hybrid perovskite (DMA= $(CH_3)_2NH_2$) was investigated.
- The two doped structures $DMACd_{0.98}Zn_{0.02}Cl_3$ and $DMACd_{0.97}Cu_{0.03}Cl_3$ were stabilized.
- The doping of the crystal with Cu^{2+} ions improves the semiconducting property of the material.
- The pure and the doped materials exhibit "cold" white light emission.
- $DMACd_{0.97}Cu_{0.03}Cl_3$ is a good visible light absorber suitable for white light emission.

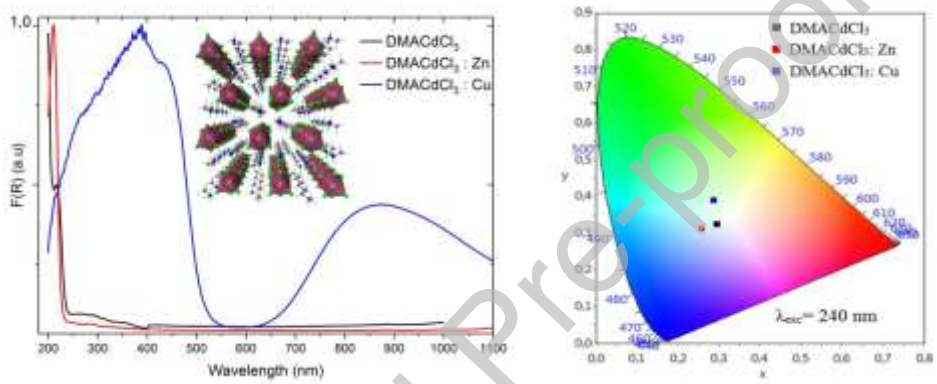

Abstract

The one-dimensional ABX_3 hybrid perovskite (A=$(CH_3)_2NH_2$=DMA, B=Cd and X=Cl) was synthesized and structurally characterized. The optical analysis showed that the material has a direct band-gap nature with a gap energy of 5.36 eV. The obtained compound exhibited a "cold" white-light emission under an excitation wavelength of 240 nm with a color-rendering index up to 92 and a correlated color temperature (CCT) of 7582 K. The doping of the crystal with Cu^{2+} ions decreased the gap energy toward 2.51 eV. The partial substitution of the Cd atoms with Cu atoms decreased the intensity of the emitted white-light under 240 nm and led to a "cold" white-light emission with a CCT of 7117 K. The doping of the material with Zn^{2+} yielded a blue-shift and the emitted light revealed a CCT of 11028 K. On the other hand, by incorporating Cu^{2+} ions into the B site a broad absorption band is observed in the visible region resulting from the d-d transitions around the copper atoms which makes the material a good visible-light absorber. Hence, the Cu doped compound could be suitable for both white-light emission and photovoltaic solar cells.

Keywords

A. optical materials, B. crystal growth, B. luminescence, B. optical properties, D. electronic structure

1. Introduction

Nowadays, hybrid molecular crystals based on metal halides have received increasing attention for their interesting biological, opto-electronic, luminescence and magnetic properties.[1–10] Organic-inorganic metal halide-based perovskites (OIMHP) are acclaimed for their electrical and opto-electrical properties.[11–20] In fact, because of their low band gap energies around 1.5 eV, the three dimensional (3-D) OIMHP are widely used in photovoltaic solar cells (SCs). The most famous 3-D OIMHP are the lead (II)-based $MAPbX_3$ ($MA = CH_3NH_3$; X = I, Br or Cl halogens) whose performance in photon conversion has been proven.[21–23] Many Several reports have shown that the gap energy and the emission properties are both tunable by varying and/or mixing the halide composition.[24] These materials are characterized with narrow emission bands at 1.6 eV (X=I), 2.32 eV (X= Br) and at 3.04 eV (X = Cl).[25,26] However, the $MAPbX_3$-based photovoltaics have demonstrated a high instability under common climate conditions, notably moisture, as well as a high toxicity due to the bioaccumulation of the lead.[27–29] Recently, researchers have suggested the substitution of Pb by other low toxic or eco-friendly metals such as Cd, Cu and Zn to develop lead-free photovoltaic devices. Unfortunately, the atomic radii of most alternatives are smaller than that of Pb atoms, which incurs low dimensional structures.[30,31] This reduction of dimensionality generates a multi quantum-well electronic structure and results in an increase of the band gap energy. In contrast with the 3D OIMHP, the low-dimensional Cd and Pb-based compounds have a great potential for white light emitter diode (WLED) applications. Meanwhile, the transition metals are suitable as light absorbers in SCs devices and the d-d transitions improve the visible light absorption. Notably, the optical and photovoltaic properties of the 2D and 1D Cu^{2+}-based perovskites are attributable to a broad-band absorption in the UV-Vis region resulting from the ligand to metal charge transfer (LMCT), and a broad Vis-NIR optical absorption corresponding to the d-d electronic transitions with the Jahn Teller distortion.[32,33] Despite their safe effect, these copper halide perovskite-based photovoltaic SCs demonstrate a lower power conversion efficiency (PCE) than the 3D perovskites. Actually, only 0.017 % is recorded for the MA_2CuCl_4.[34] In recent years, an alternative method based on the doping of the materials with transition metals was investigated to reduce the toxicity of the Pb-based photovoltaic devices. In 2018, X. Zhu et al. showed that a partial replacement of the Pb^{2+} ions with 0.01% of Zn^{2+} cations improves the photovoltaic properties of the $MAPbI_3$-based SCs with a PCE up to 15.37%.[35] As PCE reaches 16.6 %, the incorporated Zn^{2+} increases up to 0.02 %. [36] S. Thapa et al.

demonstrated that the inorganic Pb-reduced perovskite $CsZn_xPb_{1-x}I_3$ exhibits an efficient white light emission with a CRI of 93.[37] The doping of the B site in $MAPbI_3$ with Cd atoms decreases the band gap energy from 1.54 to 1.51 eV.[38] On the other hand, the experimental study of the Cu^{2+}-doped $MAPbI_3$ films confirms the usefulness of $MACu_{0.1}Pb_{0.9}I_3$ in LED and photovoltaic SCs.[39] In addition, the $CH_3NH_3PbCu_xI_{3+x}$ Cu-doped photovoltaics have shown a higher PCE compared to the non-doped $MAPbI_3$.[40] Nowadays, much effort has been deployed to study the effect of the partial substitution of the Pb atoms by transition metals on the photovoltaic properties of 3D perovskite-based absorbers. Many reports discard the photoluminescence of the 2D Cu(II)-based perovskites , however the light emission of Cu^{2+}-doped 1D perovskite remains ambiguous. Up to date, the effect of the doping of the white light emitter materials with transition metals on its photovoltaic and photoluminescent properties has not yet been exhaustively studied. In this work, a new 1D face-sharing Cd-based perovskite $DMACdCl_3$ was synthesized (DMA = $CH_3(NH_2)CH_3$). In order to modify the optical properties of the synthesized compound, we partially substituted the Cd^{2+} ions by Zn^{2+} and Cu^{2+} ions. The pure $DMACdCl_3$ and the Zn-doped $DMACdCl_3$: Zn are investigated for white light emitter (WLE) applications while the Cu-doped $DMACdCl_3$: Cu is developed for the lead-free photovoltaic SC applications. Herein, we have demonstrated that the Cu-doping change the material from WLE to a simultaneously WLE and absorber.

2. Experimental Section

2.1 Crystal growth

The $(CH_3)_2NH_2CdCl_3$ was synthesized using the $CdCl_2$ (99.99%) powder. The dimethyl amine (DMA) = $(CH_3)_2NH$ (99.99%) and HCl (48%) were purchased from Sigma Aldrich. For the synthesis of the $DMACdCl_3$ crystals, stoichiometric amounts of ammonium salt ($(CH_3)_2NH^{2+}$ Cl^-) and cadmium chloride ($CdCl_2$) were dissolved in 10 mL of water by heating under stirring for 15 min. Colorless crystals were grown after a slow evaporation of the solution at room temperature for a few days.

2.2 Instrumentation used for characterization

Full sphere data was collected on a suitable selected single crystal using a D8 VENTURE Bruker AXS diffractometer. To solve the crystal structure, we have used the direct methods and the full-matrix least squares was used to the structure refinement [41,42] on F2 with the WINGX package. [43] All details of data collection and crystal parameters are reported in table S1. The reflectance spectra were obtained using a Varian Cary 5000 UV-Visible

spectrophotometer. The steady-state photoluminescence spectra were recorded using a HORIBA FluoroMax spectrophotometer equipped with a 150 W xenon lamp.

2.3 Computational Details

All calculations have been performed using the Quantum Espresso program package.[44] Geometry optimization was carried out by keeping the experimental cell parameters fixed and relaxing only the atomic positions using the PBE exchange correlation functional [45] and a 2x2x2 k point mesh grid. We employed a monoclinic supercell containing 4 formula units with a,b,c parameters of 7.728 Å, 13.257 Å and 6.685 Å respectively and β=98.37°. We assume a Cu/Zn doping concentration of 0.25 by replacing a Cd atom in the crystal structure. The core-valence electron interactions were described using ultrasoft pseudo potentials (shells explicitly included in calculations: Cl 3s3p; N, C 2s2p; H 1s; Cd 5s5p4d; Cu 3s3p3d4s; Zn 3s3p3d4s) and a cutoff on the wavefunctions of 25 Ryd (200 Ryd on the charge density). To simulate the electronic structure, a single point calculation on the relaxed geometries has been carried out using the HSE06 functional, [46] a 2x2x2 k point mesh grid and a cutoff on the wavefunctions of 70 Ryd (280 Ryd on the charge density). For the hybrid HSE06 calculation, we adopted scalar-relativistic norm-conserving pseudo potentials with electrons from H 1s; C 2s2p; N 2s2p; Cl 3s3p; Cd 4s4p4d5s Cu 3s3p3d4s; Zn 3s3p3d4s shells explicitly included in calculations.[47] To simulate the different spin properties of the systems, all calculations were performed within the local spin density approximation by relaxing the spin multiplicity.

3. Results and discussion

3.1 Crystal structures

The single crystal X-Ray diffraction showed that the grown pure $(CH_3)_2NH_2CdCl_3$ ($DMACdCl_3$) compound crystallizes in the $P2_1/c$ space group of the monoclinic system with Z = 4. The asymmetric unit is formed with one organic cation $[CH_3NH_2CH_3]^+$ and $[CdCl_3]^-$ inorganic complex. As shown in the structure projections (**Figure 1**), the inorganic network includes mineral wires extended along the $\vec{c}$-axis. These infinite chains consist of face-shared $CdCl_6$ octahedra that lead to a 1D perovskite structure of the ABX_3 family with A= DMA, B = Cd and X = Cl. The six doubly bridging chloride ions link the adjacent Cd centers with an average Cd—Cl distance of 2.55 nm which is similar to those of a previously reported Cd(II) chloride 1D perovskite structure.[48,49] These infinite $[CdCl_3]^-_\infty$ sticks are surrounded by organic cations that are confined into the voids of the inorganic polymeric fragments and connected to the chloride anions through H-bond interactions. To investigate the structure and

the composition of the Zn-doped ($DMACdCl_3$: Zn) and the Cu-doped ($DMACdCl_3$: Zn) 1D perovskites, the single crystal X-ray diffraction (XRD) was used. The results prove the presence of the Zn and the Cu atoms inside the structures with a concentration of 2% and 3%, respectively. The doped structures were determined as $(CH_3)_2NH_2Cd_{0.98}\ Zn_{0.02}Cl_3$ and $(CH_3)_2NH_2Cd_{0.97}Cu_{0.03}Cl_3$ and they crystalize in the monoclinic crystal system with the same space group of the parent structure. All data collection and crystal parameters details are reported in **table S1**.

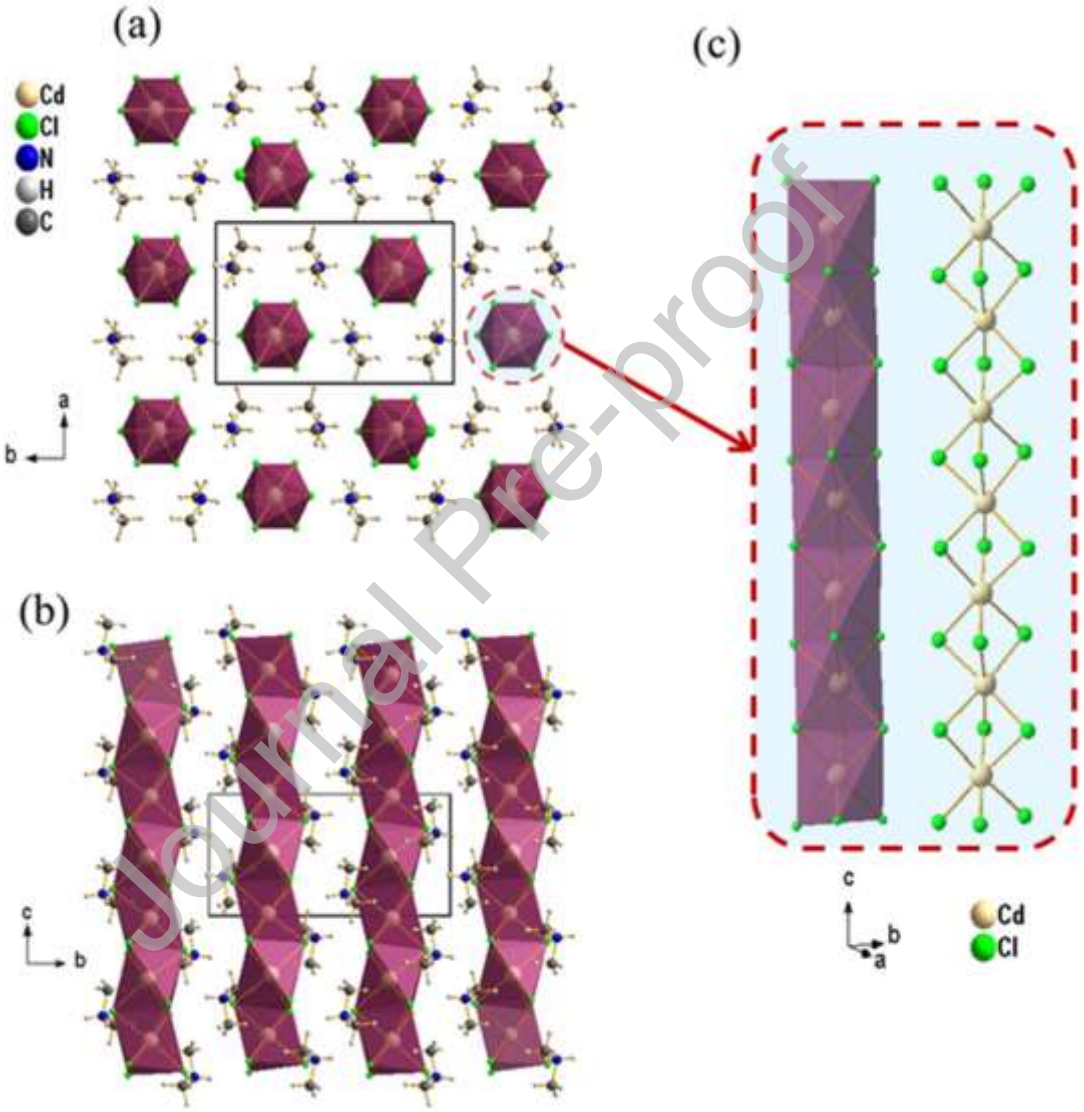

Figure 1: (a) and (b): Projections of $DMACdCl_3$ structure and (c): view of one inorganic $[\mathbf{CdCl_3}]^-_\infty$ chain

3.2 Opto-electronic properties

3.2.1 UV-Vis-NIR diffuse reflectance

The solid state diffuse reflectance spectra of the developed crystals are recorded and plotted in **Figure 2.(a)**. The doping with Zn^{2+} ions increases the reflectivity of the material in the visible region from about 50 % to 75 %. Two broad bands are observed in the spectrum of the Cu^{2+} doped compound. The first one is located between 200 and 500 nm and it corresponds to the LMCT transitions. The second one, spanning the low-energy region of the visible range and the near infrared region, results from the d-d transitions around the Cu^{2+} ions.

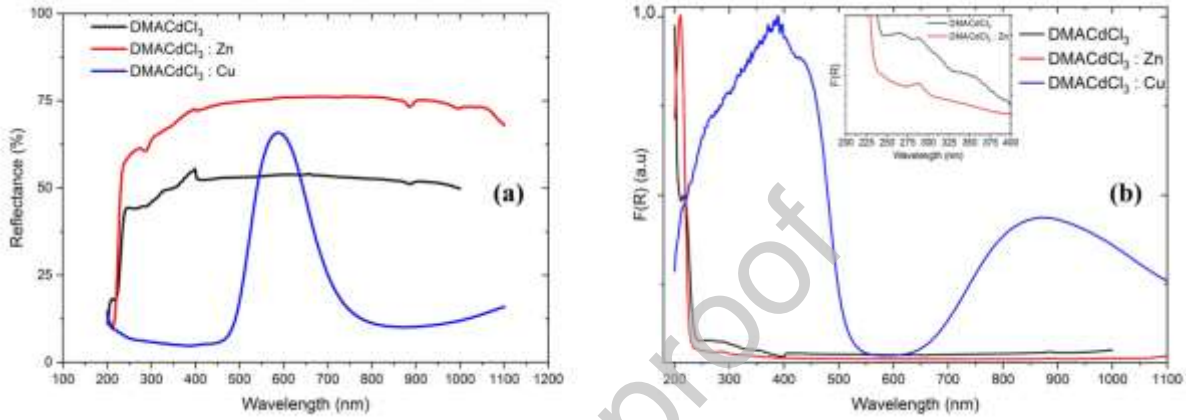

Figure 2. (a): UV-Vis-NIR diffuse reflectance spectra and (b): Kubelka-Munk absorbance spectra of $DMACdCl_3$, $DMACdCl_3$: Zn and $DMACdCl_3$: Cu.

Using the Kubelka-Munk function (Equation 1), the reflectance spectra were translated into absorption spectra (see **Figure 2.(b)**).

$$F(R) = \frac{(1-R)^2}{2R} = \frac{K}{S} \propto 2\alpha \qquad eq(1)$$

Figure 2.(b) shows no characteristic absorption in the visible range for both the pure and the Zn-doped compounds,, which makes them suitable for WLED applications. These two compounds display narrow absorption bands below 250 nm. The peaks observed between 250 and 400 nm (the inset of **Figure 2.(b)**) can be assigned to the excitons confined within the inorganic network. In the absorption spectra of the Cu^{2+}-doped compound, a large absorption band is observed in the UV-Vis range below 500 nm. This band results from the LMCT transitions within the material. The broad band in the Vis-NIR region, centered at 880 nm, results from the d-d transition within the Cu^{2+} cation. The occurrence of this band confirms

the presence of the $[CuCl_6]^{4-}$ complexes in the $DMACdCl_3$ structure. As a result, the $DMACdCl_3$: Cu material exhibits an intense absorption ranging the UV-Vis-NIR spectra, which makes it suitable as a light absorber in photovoltaic SCs. The red shift of this broad absorption band with respect to that of other transition metals, such as Mn^{2+} and Fe^{2+}, is due to the high Jahn-Teller effect around the Cu^{2+} ions in the nearly tetragonal symmetry D_{4h}. This band is observed at 884 nm in the Cu^{2+}-doped perovskite $MACdCl_4$: Cu^{2+}.[50]

The Gaussian fitting of the absorption spectrum of $DMACdCl_3$: Cu (**Figure 3**) shows that this band is an overlapping of three bands that are assigned to crystal field transitions E_1, E_2 and E_3 from a_{1g} (z^2) , b_{2g} (xy) and e_g (xz , yz) to b_{1g} (x^2-y^2), respectively. Five LMCT transitions were depicted in the UV region at 455, 397, 336, 244 and 211 nm. According to R. Valiente et al., [51] the observed bands are compared to that of the one-dimensional Cu^{2+} doped $MACdCl_3$: Cu^{2+} and assigned to their corresponding LMCT transitions (**Table 1**).

Table 1. Assignment of the observed LMCT transitions

Observed transition (nm)	Corresponding LMCT transition
455	a_{2u} (π+σ) → b_{1g} (x^2-y^2)
397	e_u (π+σ) →b_{1g} (x^2-y^2)
336	b_{2u} (π) → b_{1g} (x^2-y^2)
244	e_u (σ+π) → b_{1g} (x^2-y^2)
211	a_{2u} (σ +π) →b_{1g} (x^2-y^2)

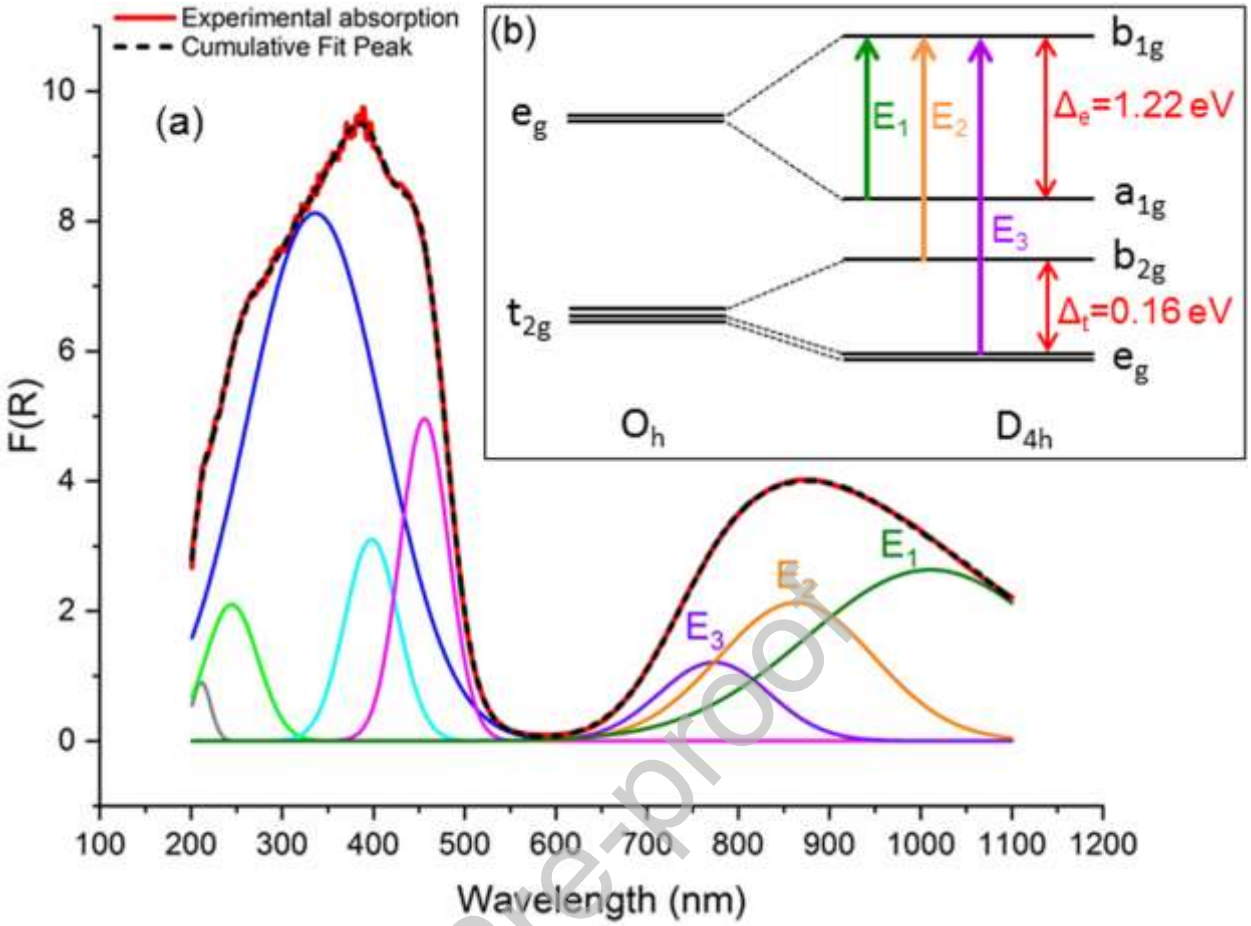

Figure 3. (a): Multi-peaks Gaussian fit of the absorption spectrum of the doped $DMACdCl_3$: Cu and (b): energetic diagram of the d-d transitions within the Cu^{2+} ion.

The fundamental band gap energies of the synthesized compounds were calculated using the Tauc relation:

$$[F(R) * h\nu]^{\frac{1}{m}} = A\,(h\nu - Eg) \qquad eq(2)$$

where A is a constant, h and ν are the Planck's constants and the photon frequency, respectively. The type of the gap transition is direct for m = 1/2 and indirect for m = 2. The calculated "m" values for the three compounds confirm the direct nature of the fundamental gap transitions inside all crystals. A detailed calculation is described in the supplementary file (Figures S1, S2 and S3). The plot of $[F(R)h\nu]^2$ vs hν (**Figure 4**) shows that the pure $DMACdCl_3$ is characterized by a large gap of 5.36 eV. This value is close to that of previously reported Cd-based halides where the conduction band (CB) arises from Cd-5s orbitals and the valence band (VB) originate from Cl-3p orbitals. [52,53]

The doping of this material by Zn^{2+} ions maintains the gap energy unchanged at about 5.61 eV while the incorporation of the transition metal Cu^{2+} decreases the gap energy towards 2.51eV.

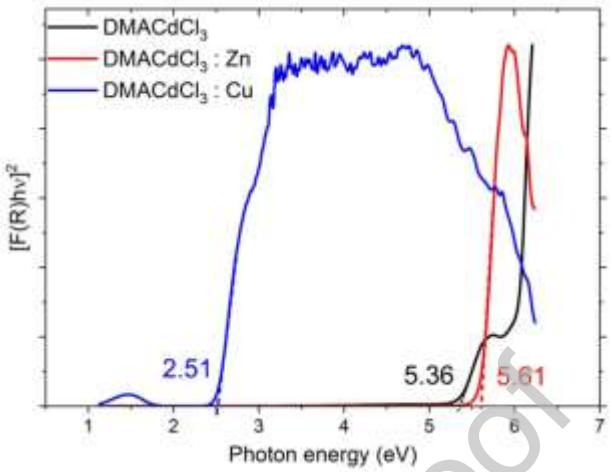

Figure 4. Tauc plots for direct gap determination.

3.2.2 Computational Modeling

To gain insight into the electronic properties of the $DMACdCl_3$-doped materials, DFT calculations have been performed, see Computational Details in Supporting Information.

Starting from the pure $DMACdCl_3$ crystal structure, we relaxed the atomic position while keeping the cell parameters fixed and we calculated a band gap of 5.58 eV in perfect agreement with the experimental measurements. Then we simulated the doped materials while replacing one of the four Cd atoms with Cu and Zn, alternatively, and proceeding to geometry relaxation and electronic structure analysis. The Cu-doped system showed a band gap of 2.62 eV while no band gap variation was found for the Zn-doped perovskite (5.59 eV) with respect to the pure Cd materials, which is in line with the optical measurements. To analyze the electronic structure, we report in **Figure 5** the density of states (DOS) for the simulated species. In particular, the pure Cd perovskite shows a VB mainly constituted by the Cl contribution while the CB is associated to the Cd states coupled with the Cl contribution (see **Figure 5.(a)**). As for the doped material, while the VB is also associated in these cases to the Cl contributions, the Cu atoms introduce an unoccupied state in the $DMACdCl_3$: Cu perovskite that causes the lowering of the band gap at 2.62 eV, see **Figure 5.(b)**. On the other hand, the Zn-doped system shows a CB with the Cd contribution coupled with Zn states at a

slightly higher energy, see **Figure 5.(c)**. For all three systems, organic contribution is shallow in the VB and CB.

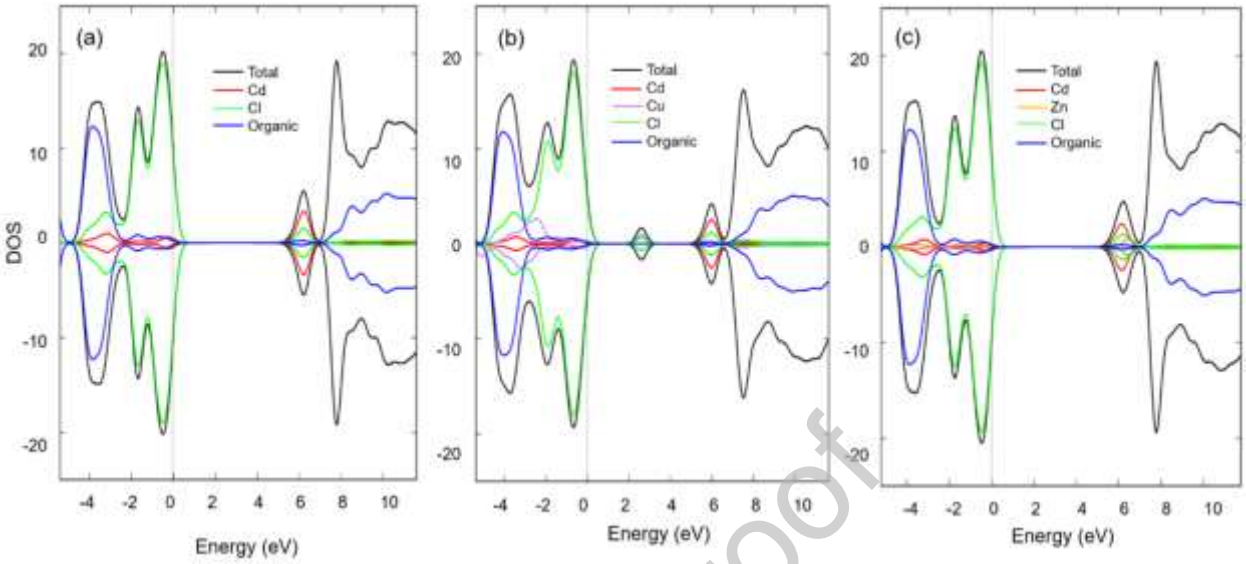

Figure 5. Density of States (DOS) with metal contribution, chloride contribution and spin differentiation (α positive, β negative) of (a) $DMACdCl_3$, (b) Cu: $DMACdCl_3$ and (c) Zn: $DMACdCl_3$.

3.2.3 Photoluminescence properties

Recently, the white light emission from Cd-based low-dimensional structures have been demonstrated.[52,53] In previously reported Cd-based halides, the emission analysis has shown that the PL properties are very similar to those of the pure CdX_2 (X = Br, Cl and I). [14,54,55] The emission peaks of the pure CdX_2 compounds are observed in the range 326-620 nm and their positions depend on the halogen nature and the excitation wavelength.[56–60] In order to study the effect of the partial substitution of Cd atoms with Zn and Cu atoms on the luminescence properties of the $DMACdCl_3$, the pure and the doped materials were first excited with photon energy above the gap energy of the pure $DMACdCl_3$ under 6.2 eV (λ_{exc}= 200 nm). Then, they were excited below the gap, under 5.16 eV (240 nm). As shown in **Figure 6**, all the compounds exhibited a broad-band emission spanning hole in the visible range and the emission intensity decreases substantially by the substitution of Cd atoms. The

multi-peaks deconvolution of the emission spectra of the pure $DMACdCl_3$ obtained under 200 nm and 240 nm shows that the observed PL band results from two bands centered at 382 and 522 nm under an excitation wavelength of 200 nm and at 335 and 508 nm under 240 nm (**Figure 7**). According to previously studied Cd-based hybrid compounds, the higher energy band is assigned to photo-induced excitons confined within the inorganic $CdCl_6$ octahedra while the lowest energy broad band results from the self-trapped excitons (STE) transitions. [52,53] **Figures 8** and **9** show the multi-peaks fitting of the PL spectra of the doped materials excited under 200 and 240 nm. It is clear that the doping of the material generates a slight shift of these peaks.

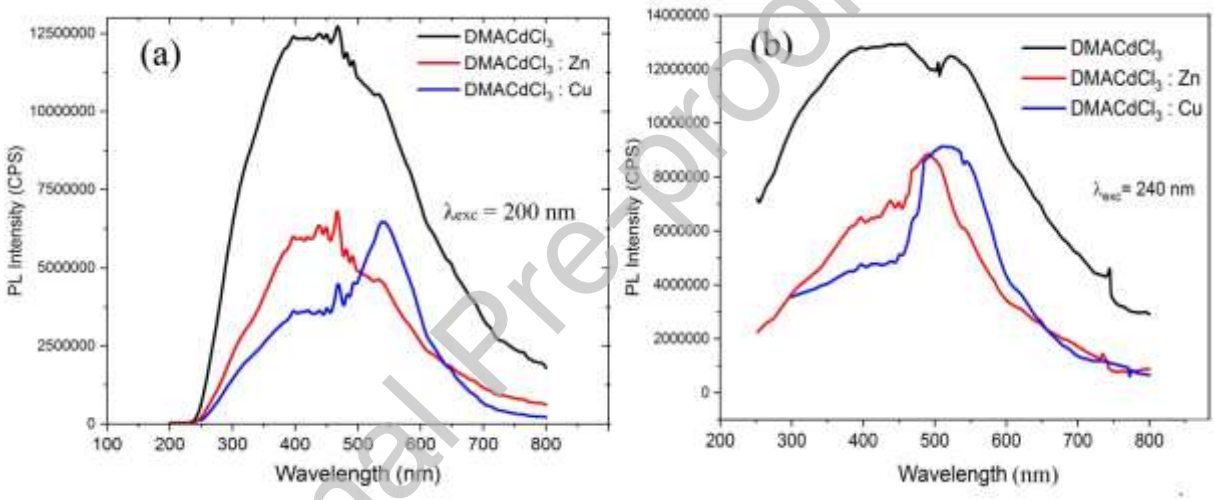

Figure 6. PL spectra of the pure and the doped compounds under excitation wavelength of 200 nm (a) and 240 nm (b).

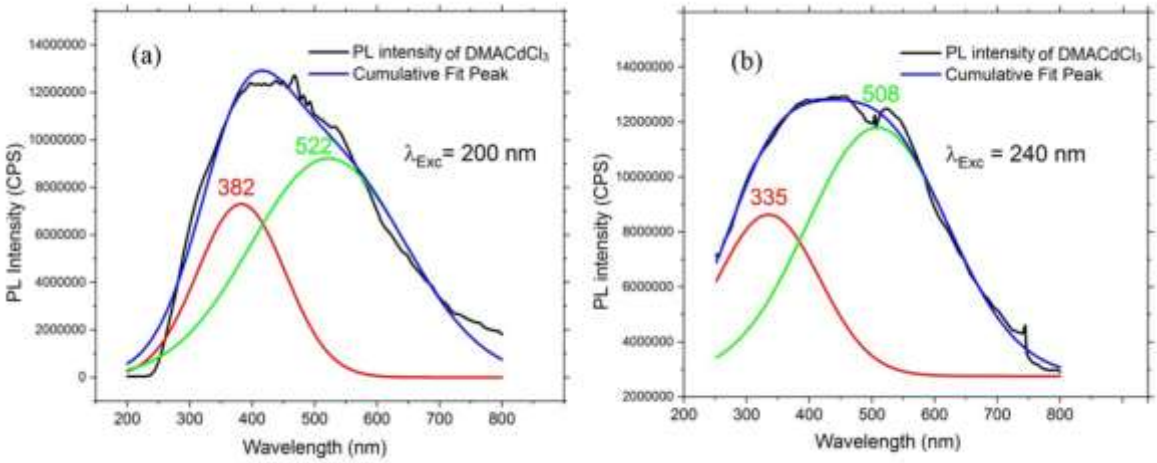

Figure 7. Multi-peaks fitting of the experimental PL spectra of the pure $DMACdCl_3$ under excitation wavelength of 200 nm (a) and 240 nm (b).

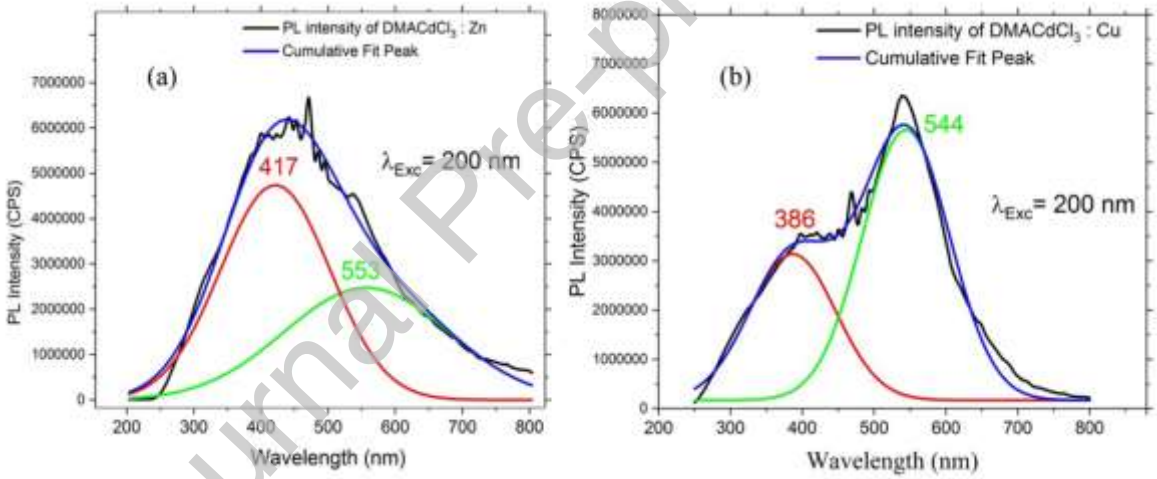

Figure 8. Multi-peaks fitting of the experimental PL spectra of (a): the Zn-doped and (b): the Cu-doped compounds under λ_{Exc} = 200 nm.

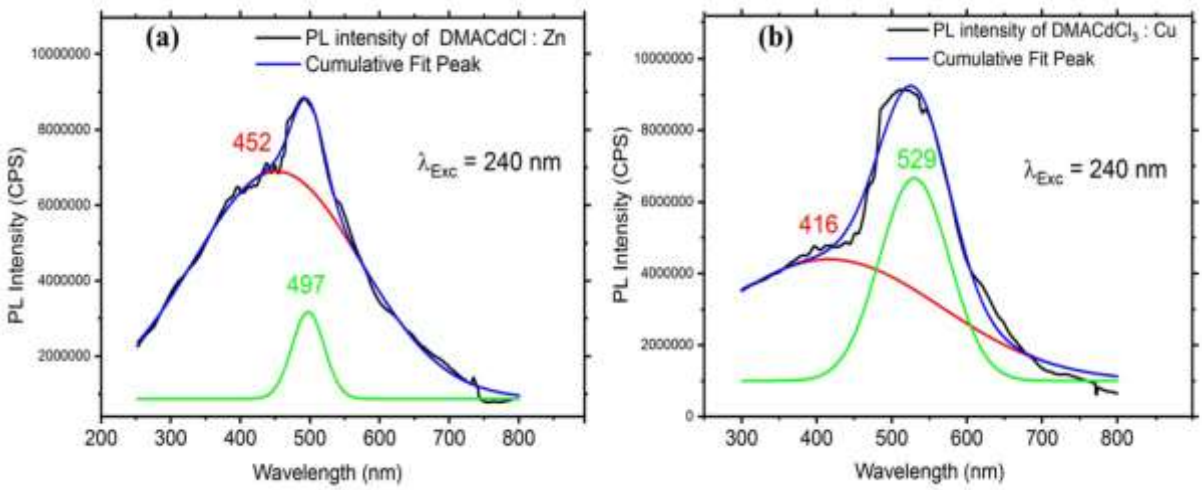

Figure 9. Multi-peaks fitting of the experimental PL spectra of the Zn-doped (a) and the Cu-doped (b) compounds under λ_{Exc} = 240 nm.

The calculated chromaticity coordinates CIE are visualized on the chromaticity diagram 1931 (Figure 10). All the calculated parameters ((x ; y), CRI and Correlated Color Temperature (CCT)) characteristic of the emitted light under 200 and 240 nm are presented in Table 2. The pure $DMACdCl_3$ exhibited the greater color rendering index (CRI) above 90. The doping of the parent structure leads to the diminution of the CRI. With CCT above 6500 K, all the compounds show "cold" white light emission. Compared to the emission of the pure $DMACdCl_3$, the doping of the parent material by Zn^{2+} ions shifts the emission to the blue side whereas the incorporation of Cu^{2+} shifts emission to the green side. As a result, the pure $DMACdCl_3$ and the Zn-doped compounds are suitable for optoelectronic and WLED applications. For the Cu^{2+} doped $DMACdCl_3$: Cu perovskite, we demonstrate its suitability for both light emission and light absorber applications.

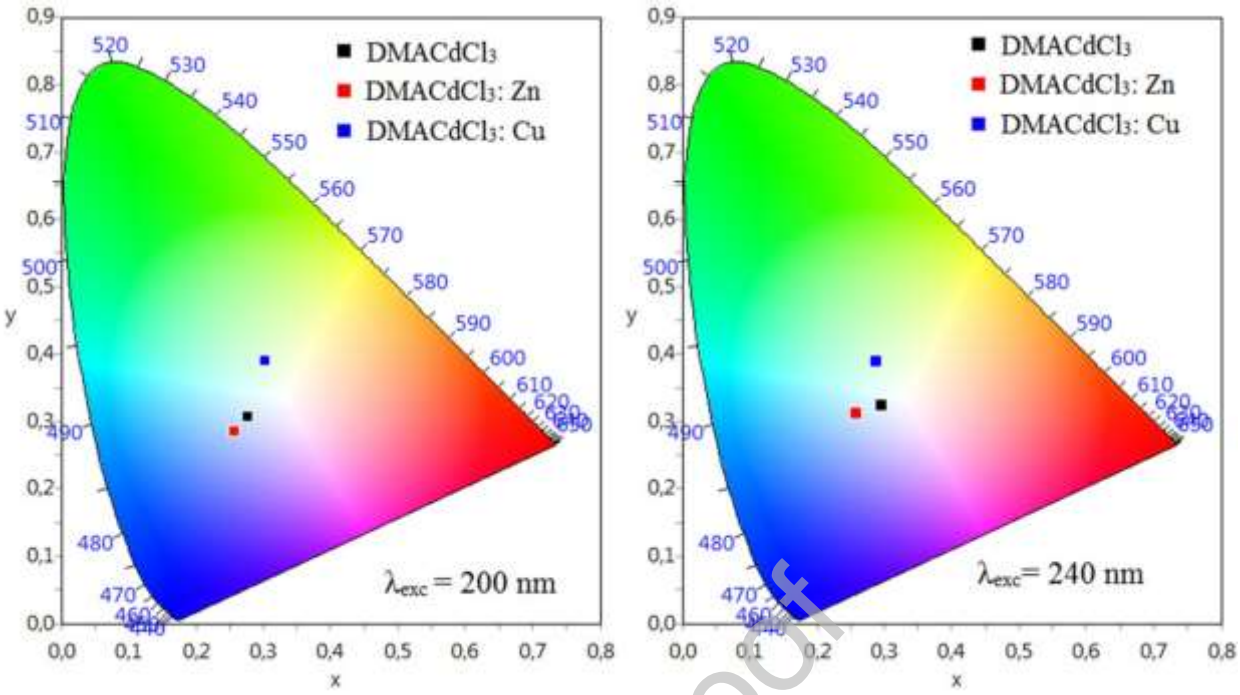

Figure 10 : CIE color coordinates of the emitted light in the 1931 chromaticity diagram: (a) under λ_{Exc}=200 nm and (b) under λ_{Exc}=240 nm.

Table 1. The chromaticity coordinates (x,y), the correlated color temperatures (CCT) and color rendering index (CRI).

λ_{Exc} (nm)	Compound	(x,y)	CRI	CCT [K]
200	$DMACdCl_3$	(0.27 ; 0.30)	91	9384
	$DMACdCl_3$: Zn	(0.25 ; 0.28)	89	13270
	$DMACdCl_3$: Cu	(0.30 ; 0.38)	69	6540
240	$DMACdCl_3$	(0.29 ; 0.32)	92	7582
	$DMACdCl_3$: Zn	(0.25 ; 0.31)	84	11028
	$DMACdCl_3$: Cu	(0.28 ; 0.38)	71	7117

4. Conclusions

In this paper, the one-dimensional $DMACdCl_3$ hybrid perovskite (DMA= $(CH_3)_2NH_2$) was investigated and structurally characterized. In order to study the effect of the material doping with Zn^{2+} and Cu^{2+} ions on its optical and electronic behaviors, the two doped structures $DMACd_{0.98}Zn_{0.02}Cl_3$ and $DMACd_{0.97}Cu_{0.03}Cl_3$ were successfully stabilized. The UV-Vis-NIR absorption analysis shows that the pure material has a direct band gap nature with a gap energy of 5.36 eV. While the doping of the crystal with Cu^{2+} ions decreases the gap energy toward 2.51 eV, improving the semiconducting property of the material, the gap energy of the Zn^{2+} doped material is unchanged. The $DMACdCl_3$ exhibits "cold" white light emission under an excitation wavelength of 240 nm with a CRI up to 92 and a correlated color temperature (CCT) of 7582 K. The partial substitution of the Cd atoms with Cu atoms decreases the intensity of the emitted white light under 240 nm and leads to "cold" white light emission with a CRI of about 71 and a CCT of 7117 K. By the doping of the material with Zn^{2+} ions, a blue-shift is observed, and the emitted light exhibits a CRI of 84 and a CCT about 11028 K. Then, the incorporation of Cu^{2+} ions into the structure makes the material suitable for WLE and photovoltaic SC applications with an enhancement of the visible light absorbance thanks to the d-d transitions within the Cu^{2+} cations.

H. N., H. S., A. T. and NA. A. contributed to the conceptualization, funding acquisition and supervision of the study; S. E., R. M. and H. N. contributed to the optical and the PL properties; H. J. carried out the synthesis and the crystals growth; T. R. performed the structural characterization and E. M. investigated the quantum calculations and computational data.

Conflicts of interest

There are no conflicts to declare.

Acknowledgements

The authors extend their appreciation to the Deputyship for Research & Innovation, Ministry of Education in Saudi Arabia for funding this work through the project number "375213500". The authors would like to extend their sincere appreciation to the central laboratory at Jouf University for supporting this study.

References

[1] S. Dgachi, A.M. Ben Salah, M.M. Turnbull, T. Bataille, H. Naïli, Investigations on (C6H9N2)2[MIIBr4] halogenometallate complexes with MII = Co, Cu and Zn: Crystal structure, thermal behavior and magnetic properties, J. Alloys Compd. 726 (2017) 315–322. doi:10.1016/j.jallcom.2017.07.278.

[2] R. Jlassi, A.P.C. Ribeiro, M. Mendes, W. Rekik, G.A.O. Tiago, K.T. Mahmudov, H. Naïli, M.F.C. Guedes da Silva, A.J.L. Pombeiro, Arylhydrazone Cd(II) and Cu(II) complexes as catalysts for secondary alcohol oxidation, Polyhedron. 129 (2017) 182–188. doi:10.1016/j.poly.2017.03.020.

[3] O. Kammoun, H. Naïli, W. Rekik, T. Bataille, Layered structure of a supramolecular hybrid sulfate salts: Thermal stability and magnetic behavior, Inorganica Chim. Acta. 434 (2015) 209–214. doi:10.1016/j.ica.2015.05.031.

[4] W. Rekik, H. Naïli, T. Mhiri, T. Bataille, Three organically templated magnesium sulfates: Chemical preparation, hydrogen-bonded structures and thermal behavior, Solid State Sci. 14 (2012) 1503–1511. doi:10.1016/j.solidstatesciences.2012.08.027.

[5] N.L. Nkhili, W. Rekik, H. Naïli, T. Mhiri, T. Bataille, Piperazinediium diselenatohexaaquacobaltate(II) dihydrate (C4H12N2)[Co(SeO4)2(H2O)4]·2H2O, Solid State Phenom. 194 (2013) 171–174. doi:10.4028/www.scientific.net/SSP.194.171.

[6] N.L. Nkhili, W. Rekik, H. Naïli, A new nickel selenate templated by piperazine: Chemical preparation, crystal structure, thermal decomposition, and magnetic properties, Monatshefte Fur Chemie. 145 (2014) 931–936. doi:10.1007/s00706-014-1151-7.

[7] S. Walha, H. Naïli, S. Yahyaoui, B.F. Ali, M.M. Turnbull, T. Mhiri, S.W. Ng, Three-dimensional network polymeric structure of (2-amino-5 ammoniopyridinium)[CuCl4]: Crystal supramolecularity and magnetic properties, J. Supercond. Nov. Magn. 26 (2013) 437–442. doi:10.1007/s10948-012-1759-y.

[8] A. Piecha, A. Gągor, M. Węcławik, R. Jakubas, W. Medycki, Anomalous dielectric behaviour in centrosymmetric organic-inorganic hybrid chlorobismuthate(III) containing functional N,N-dimethylethylammonium ligand. Crystal structure and properties, Mater. Res. Bull. 48 (2013) 151–157. doi:10.1016/j.materresbull.2012.10.018.

[9] R. Elwej, M. Hamdi, N. Hannachi, F. Hlel, Temperature- and frequency-dependent dielectric properties of organic-inorganic hybrid compound: (C6H9N2)2(Hg0.75Cd0.25)Cl4, Mater. Res. Bull. 62 (2015) 42–51. doi:10.1016/j.materresbull.2014.10.074.

[10] S. Elleuch, I. Triki, Y. Abid, Optical and charge transfer properties of a new cadmium based metal-organic-framework material, Mater. Res. Bull. 150 (2022) 111754. doi:https://doi.org/10.1016/j.materresbull.2022.111754.

[11] X. Jiang, Z. Chen, X. Tao, (1-C5H14N2Br) 2 MnBr 4 : A Lead-Free Halide With Intense Green Photoluminescence, Front. Chem. 8 (2020) 2–9. doi:10.3389/fchem.2020.00352.

[12] D. Shanthi, P. Selvarajan, S. Perumal, Growth, linear optical constants and photoluminescence characteristics of beta-alaninium picrate (BAP) crystals, Optik (Stuttg). 127 (2016) 3192–3199. doi:10.1016/j.ijleo.2015.11.189.

[13] C. Deng, G. Zhou, D. Chen, J. Zhao, Y. Wang, Q. Liu, Physical Insights into Light Interacting with Matter Broadband Photoluminescence in 2D Organic – Broadband Photoluminescence in 2D Organic – Inorganic Hybrid, J. Phys. Chem. Lett. 11 (2020) 2934–2940. doi:10.1021/acs.jpclett.0c00578.

[14] R. Roccanova, M. Houck, A. Yangui, D. Han, H. Shi, Y. Wu, D.T. Glatzhofer, D.R. Powell, S. Chen, H. Fourati, A. Lusson, K. Boukheddaden, M. Du, B. Saparov, Broadband Emission in Hybrid Organic – Inorganic Halides of Group 12 Metals, ACS Omega. 3 (2018) 18791–18802. doi:10.1021/acsomega.8b02883.

[15] P. Zawal, H. Sen, S. Klejna, T. Mazur, E. Wlaz, K. Szaciłowski, Halogen-containing semiconductors : From artificial photosynthesis to unconventional computing, Coord. Chem. Rev. 415 (2020) 213316. doi:10.1016/j.ccr.2020.213316.

[16] C. Zhou, H. Lin, Q. He, L. Xu, M. Worku, M. Chaaban, Low dimensional metal halide perovskites and hybrids, Mater. Sci. Eng. R. 137 (2019) 38–65. doi:10.1016/j.mser.2018.12.001.

[17] J. Wang, Y. Liu, S. Han, Y. Li, Z. Xu, J. Luo, M. Hong, Z. Sun, Y. Liu, S. Han, Y. Li, Z. Xu, J. Luo, M. Hong, Z. Sun, Ultrasensitive polarized-light photodetectors based on 2D hybrid, Sci. Bull. 66 (2020) 158–163. doi:10.1016/j.scib.2020.06.018.

[18] R. Msalmi, S. Elleuch, B. Hamdi, E. Radicchi, A. Tozri, H. Naïli, M.R. Berber, Tunable broad-band white-light emission in two-dimensional (110)-oriented lead bromide perovskite (C 3 H 8 N 6)[PbBr 4]: optical, electronic and luminescence properties , New J. Chem. 45 (2021) 20850–20859. doi:10.1039/d1nj03838a.

[19] K. Nageswara Rao, A. Singh, G. Vijaya Prakash, Synthesis, structure and optical studies of inorganic-organic hybrid semiconductor, (H3NC6H4CH2NH 3) PbI4, Mater. Res. Bull. 52 (2014) 78–81. doi:10.1016/j.materresbull.2013.12.063.

[20] N. Kawano, A. Horimoto, H. Kimura, D. Nakauchi, M. Akatsuka, T. Yanagida, Radiation response characteristics of organic–inorganic perovskite-type compounds with a chlorophenethylamine, Mater. Res. Bull. 142 (2021) 111409. doi:10.1016/j.materresbull.2021.111409.

[21] A. Kojima, K. Teshima, Y. Shirai, T. Miyasaka, Organometal Halide Perovskites as

Visible-Light Sensitizers for Photovoltaic, JACS Commun. (2009) 6050–6051. doi:10.1021/ja809598r.

[22] T.M. Koh, K. Fu, Y. Fang, S. Chen, T.C. Sum, N. Mathews, S.G. Mhaisalkar, P.P. Boix, T. Baikie, Formamidinium-containing metal-halide: An alternative material for near-IR absorption perovskite solar cells, J. Phys. Chem. C. 118 (2014) 16458–16462. doi:10.1021/jp411112k.

[23] Y.H. Khattak, E. Vega, F. Baig, B.M. Soucase, Performance investigation of experimentally fabricated lead iodide perovskite solar cell via numerical analysis, Mater. Res. Bull. 151 (2022) 111802. doi:https://doi.org/10.1016/j.materresbull.2022.111802.

[24] S. Adjokatse, H.H. Fang, M.A. Loi, Broadly tunable metal halide perovskites for solid-state light-emission applications, Mater. Today. 20 (2017) 413–424. doi:10.1016/j.mattod.2017.03.021.

[25] Z.K. Tan, R.S. Moghaddam, M.L. Lai, P. Docampo, R. Higler, F. Deschler, M. Price, A. Sadhanala, L.M. Pazos, D. Credgington, F. Hanusch, T. Bein, H.J. Snaith, R.H. Friend, Bright light-emitting diodes based on organometal halide perovskite, Nat. Nanotechnol. 9 (2014) 687–692. doi:10.1038/nnano.2014.149.

[26] N. Kitazawa, Y. Watanabe, Y. Nakamura, Optical properties of CH3NH3PbX3 (X = halogen) and their mixed-halide crystals, J. Mater. Sci. 37 (2002) 3585–3587. doi:10.1023/A:1016584519829.

[27] B. Conings, J. Drijkoningen, N. Gauquelin, A. Babayigit, J. D'Haen, L. D'Olieslaeger, A. Ethirajan, J. Verbeeck, J. Manca, E. Mosconi, F. De Angelis, H.G. Boyen, Intrinsic Thermal Instability of Methylammonium Lead Trihalide Perovskite, Adv. Energy Mater. 5 (2015) 1–8. doi:10.1002/aenm.201500477.

[28] T. Leijtens, G.E. Eperon, N.K. Noel, S.N. Habisreutinger, A. Petrozza, H.J. Snaith, Stability of metal halide perovskite solar cells, Adv. Energy Mater. 5 (2015) 1–23. doi:10.1002/aenm.201500963.

[29] A. Babayigit, A. Ethirajan, M. Muller, B. Conings, Toxicity of organometal halide perovskite solar cells, Nat. Mater. 15 (2016) 247–251. doi:10.1038/nmat4572.

[30] C. Li, X. Lu, W. Ding, L. Feng, Y. Gao, Z. Guo, Formability of ABX 3 (X = F, Cl, Br, I) halide perovskites, Acta Crystallogr. Sect. B Struct. Sci. 64 (2008) 702–707. doi:10.1107/S0108768108032734.

[31] C. Li, K.C.K. Soh, P. Wu, Formability of ABO3 perovskites, J. Alloys Compd. 372 (2004) 40–48. doi:10.1016/j.jallcom.2003.10.017.

[32] M. Bourwina, R. Msalmi, S. Walha, M.M. Turnbull, T. Roisnel, F. Costantino, E. Mosconi, H. Naïli, A new lead-free 1D hybrid copper perovskite and its structural, thermal, vibrational, optical and magnetic characterization, J. Mater. Chem. C. 9 (2021) 5970–5976. doi:10.1039/d0tc05948j.

[33] R. Valiente, F. Rodriguez, Comment on 'copper-Substituted Lead Perovskite Materials Constructed with Different Halides for Working (CH3NH3)2CuX4-Based Perovskite Solar Cells from Experimental and Theoretical View', ACS Appl. Mater. Interfaces. 12 (2020) 37807–37810. doi:10.1021/acsami.0c11480.

[34] D. Cortecchia, H.A. Dewi, J. Yin, A. Bruno, S. Chen, T. Baikie, P.P. Boix, M. Gra, Lead-Free MA 2 CuCl x Br 4-x Hybrid Perovskites, Inorg. Chem. 55 (2016) 1044–1052. doi:10.1021/acs.inorgchem.5b01896.

[35] X.-Y. Zhu, M.-W. Chen, B. Wang, N. Liu, M.-K. Ran, H. Yang, Y.-P. Yang, Improved photovoltaic properties of nominal based perovskite solar cells, Opt. Express. 26 (2018) 984–995.

[36] M. Que, W. Chen, P. Chen, J. Liu, X. Yin, B. Gao, W. Que, Effects of Zn2+ ion doping on hybrid perovskite crystallization and photovoltaic performance of solar cells, Chem. Phys. 517 (2019) 80–84. doi:10.1016/j.chemphys.2018.09.032.

[37] S. Thapa, G.C. Adhikari, H. Zhu, A. Grigoriev, P. Zhu, Zn-Alloyed All-Inorganic Halide Perovskite-Based White Light-Emitting Diodes with Superior Color Quality, Sci. Rep. 9 (2019) 18636. doi:10.1038/s41598-019-55228-1.

[38] R.K. Singh, R. Kumar, N. Jain, M.T. Kuo, C.P. Upadhyaya, J. Singh, Exploring the impact of the Pb2+ substitution by Cd2+ on the structural and morphological properties of CH3NH3PbI3 perovskite, Appl. Nanosci. 9 (2019) 1953–1962. doi:10.1007/s13204-019-01021-5.

[39] X. Ge, X. Qu, L. He, Y. Sun, X. Guan, Z. Pang, C. Wang, L. Yang, F. Wang, F. Rosei, 3D low toxicity Cu-Pb binary perovskite films and their photoluminescent/photovoltaic performance, J. Mater. Chem. A. 7 (2019) 27225–27235. doi:10.1039/c9ta12736d.

[40] Y. Shirahata, T. Oku, Photovoltaic properties of Cu-doped CH3NH3PbI3 with perovskite structure, AIP Conf. Proc. 1807 (2017) 020008. doi:10.1063/1.4974790.

[41] G.. Sheldrick, SHELXS97, Program for the Solution of Crystal Structures, A Short Hist. SHELX. (2008).

[42] G.M. Sheldrick, SHELXL97. Program for the Refinement of Crystal Structures, Acta. Cryst. A64 (2008) 112–122. doi:10.1177/004057368303900411.

[43] L.J. Farrugia, WinGX and ORTEP for Windows: An update, J. Appl. Crystallogr. 45 (2012) 849–854. doi:10.1107/S0021889812029111.

[44] P. Giannozzi, S. Baroni, N. Bonini, M. Calandra, R. Car, C. Cavazzoni, D. Ceresoli, G.L. Chiarotti, M. Cococcioni, I. Dabo, A. Dal Corso, S. De Gironcoli, S. Fabris, G. Fratesi, R. Gebauer, U. Gerstmann, C. Gougoussis, A. Kokalj, M. Lazzeri, L. Martin-Samos, N. Marzari, F. Mauri, R. Mazzarello, S. Paolini, A. Pasquarello, L. Paulatto, C. Sbraccia, S. Scandolo, G. Sclauzero, A.P. Seitsonen, A. Smogunov, P. Umari, R.M. Wentzcovitch, QUANTUM ESPRESSO: A modular and open-source software project for quantum simulations of materials, J. Phys. Condens. Matter. 21 (2009) 395502. doi:10.1088/0953-8984/21/39/395502.

[45] J.P. Perdew, K. Burke, M. Ernzerhof, Generalized gradient approximation made simple, Phys. Rev. Lett. 77 (1996) 3865–3868. doi:10.1103/PhysRevLett.77.3865.

[46] J. Heyd, G.E. Scuseria, M. Ernzerhof, Hybrid functionals based on a screened Coulomb potential, J. Chem. Phys. 118 (2003) 8207–8215. doi:10.1063/1.1564060.

[47] E. Van Lenthe, E.J. Baerends, J.G. Snijders, Relativistic regular two-component Hamiltonians, J. Chem. Phys. 99 (1993) 4597–4610. doi:10.1063/1.466059.

[48] Z. Aurang, S. Zhihua, K. Tariq, A. Muhammad Adnan, W. Zhenyue, L. Lina, C. Ji, J. Luo, [C5H12N]CdCl3: An ABX3 Perovskite–type Semiconducting Switchable Dielectric Phase Transition Material Aurang, Inorg. Chem. 11 (1914) 34–62. doi:10.1039/AR9141100034.

[49] R. Puget, M. Jannin, C. De Brauer, R. Perret, Structures oftrimethyloxosulfonium salts. V. The catena-tri-μ-chloro- cadmate and the catena-tri-μ-bromo-cadmate, Acta Crystallogr. Sect. C Cryst. Struct. Commun. 47 (1991) 1803–1805. doi:10.1107/S0108270190013701.

[50] R. Valiente, F. Rodriguez, POLARIZED ELECTRONIC SPECTRA OF THE (CH3NH3) 2Cd ,_, Mn , C14 (x = O-l) PEROVSKITE LAYER DOPED WITH Cu2 + : STUDY OF THE Cl- + Cu2 + CHARGE TRANSFER INTENSITY ENHANCEMENT ALONG THE SERIES b (A), J. Phys. Chem. Solids. 57 (1996) 571–587.

[51] R. Valiente, M.C.M. de Lucas, F. Rodriguez, Polarized charge transfer spectroscopy of Cu 2 + in doped one-dimensional [N (CH 3) 4] CdCl 3 and Polarized charge transfer spectroscopy of Cu2 + in doped one-dimensional [N (CH3) 4] CdCl3 and [N (CH3) 4] CdBr3 crystals, J. Phys. Condens. Matter. 6 (1994) 4527–4540.

[52] W. Sasa, L. Li, Z. Sun, C. Ji, S. Liu, Z. Wu, S. Zhao, M. Hong, J. Luo, A semi-conductive organic-inorganic hybrid emits pure white light with ultrahigh color rendering index, J. Mater. Chem. C. 5 (2017) 4731–4735. doi:10.1039/C7TC00279C.

[53] Z. Qi, Y. Chen, Y. Guo, X. Yang, F.Q. Zhang, G. Zhou, X.M. Zhang, Broadband white-light emission in a one-dimensional organic-inorganic hybrid cadmium chloride with face-sharing CdCl6octahedral chains, J. Mater. Chem. C. 9 (2021) 88–94. doi:10.1039/d0tc04731g.

[54] A. Ohnishi, T. Yamada, T. Yoshinari, I. Akimoto, K. Kanno, T. Kamikawa, Emission Spectra and Decay Characteristics in Photo-Stimulated (CnH2n+,NHa)2CdCh : n=l, 2, 3, J. Electron Spectros. Relat. Phenomena. 79 (1996) 163–166.

[55] R. Roccanova, W. Ming, V.R. Whiteside, M. AMcGuire, I.R. Sellers, M. Du And, B. Saparov, Synthesis, Crystal and Electronic Structures, and Optical Properties of (CH3NH3)2CdX4 (X = Cl, Br, I), Inorg. Chem. 56 (2017) 13878–13888. doi:10.1021/acs.inorgchem.7b01986.

[56] A. Ohnishi, M. Kitaura, H. Nakagawa, Determination of Optical Gain of Self-Trapped Exciton Luminescence in CdI2, J. Phys. Soc. Japan. 63 (1994) 4648–4654.

[57] H. Nakagawa, K. Hayashi, H. Matsumoto, Luminescence od CdCl2-CdBr Solid Solution, J. Phys. Soc. Jpn. 43 (1977) 1655–1663.

[58] H. Matsumoto, H. Nakagawa, RELAXED EXCITONIC STATES IN Cd!2 CRYSTALS Hiroaki MATSUMOTO and Hideyuki NAKAGAWA, J. Lumin. 18/19 (1979) 19–22.

[59] T. Hayashi, T. Ohata, S. Koshino, INDIRECT EXCITON LUMINESCENCE AND RAMAN SCATTERING IN Cdl2, Solid State Commun. 38 (1981) 845–847.

[60] M. Kitaura, A. Nakawa, K. Fukui, M. Fujita, T. Miyanaga, W. Makoto, Decay Time Studies on UV-Luminescence in CdBr2-CdCI Mixed Crystals, J. Electron Spectros.

Relat. Phenomena. 79 (1996) 175–178.